ENVIRONMENTAL RESEARCH
LETTERS

LETTER • OPEN ACCESS

Sensitivity of regional monsoons to idealised equatorial volcanic eruption of different sulfur emission strengths

To cite this article: Roberta D'Agostino and Claudia Timmreck 2022 *Environ. Res. Lett.* **17** 054001

IOP Publishing Environ. Res. Lett. 17 (2022) 054001 https://doi.org/10.1088/1748-9326/ac62af

ENVIRONMENTAL RESEARCH
LETTERS

LETTER

Sensitivity of regional monsoons to idealised equatorial volcanic eruption of different sulfur emission strengths

Roberta D'Agostino* and **Claudia Timmreck**

Max Planck Institut für Meteorologie, Hamburg, Germany
* Author to whom any correspondence should be addressed.

E-mail: roberta.dagostino@mpimet.mpg.de

Keywords: monsoons, volcanic forcing, grand ensemble, internal variability, Pinatubo

Supplementary material for this article is available online

OPEN ACCESS

RECEIVED
1 December 2021

REVISED
24 March 2022

ACCEPTED FOR PUBLICATION
30 March 2022

PUBLISHED
19 April 2022

Abstract

The impact of volcanic forcing on tropical precipitation is investigated in a new set of sensitivity experiments within the Max Planck Institute Grand Ensemble framework. Five ensembles are created, each containing 100 realizations for an idealized 'Pinatubo-like' equatorial volcanic eruption with emissions covering a range of 2.5-40 Tg sulfur (S). The ensembles provide an excellent database to disentangle the influence of volcanic forcing on monsoons and tropical hydroclimate over the wide spectrum of the climate's internal variability. Monsoons are generally weaker for two years after volcanic eruption and their weakening is a function of emissions. However, only a stronger than Pinatubo-like eruption ($\geqslant$10 Tg S) leads to significant and substantial monsoon changes, and some regions (such as North and South Africa, South America and South Asia) are much more sensitive to this kind of forcing than the others. The decreased monsoon precipitation is strongly tied to the weakening of the regional tropical overturning. The reduced atmospheric net energy input and increased gross moist stability at the Hadley circulation updraft due to the equatorial volcanic eruption, require a slowdown of the circulation as a consequence of less moist static energy exported away from the intertropical convergence zone.

1. Introduction

Volcanic eruptions are one of the most important natural drivers of climate variability and can significantly impact global and regional hydroclimate from several years up to decades (e.g. [1, 2]). Sulfur gases injected into the stratosphere by large explosive eruptions form sulfate aerosol particles which reflect the incoming shortwave solar radiation resulting in cooling of Earth's surface. In addition, they absorb solar near-infrared and terrestrial infrared radiation, leading to a warming of the lower-to-mid stratosphere. Hence, large explosive volcanic eruptions impact the atmospheric energy budget, and consequently the hydrological cycle: the atmospheric circulation responds to volcanic-induced energy budget changes [3] following the 'wet-gets-wetter, dry-gets-drier' paradigm, but with reversed signs than usually seen under global warming [4–6].

Monsoon systems are particularly sensitive to this kind of forcing because the atmospheric circulation and moisture convergence are constrained by energy budget changes and net energy input (NEI) zonal asymmetries [7, 8]: in fact, the shortwave reflection and the consequent radiative cooling suppress clouds and weakens the deep tropical convection and the rising branch of the Hadley circulation [9–13]. Furthermore, the atmospheric circulation shifts meridionally depending on the latitude of the eruptions, so that monsoons and the intertropical convergence zone (ITCZ) have an inter-hemispherically asymmetric response: for a Northern Hemisphere (NH) volcanic eruption, the ITCZ shifts southward [10, 14, 15] and monsoons weaken in the NH, but enhance in the Southern Hemisphere (SH [3]). This could lead to strong regional hydroclimate impacts: For example, the inter-hemispheric asymmetric precipitation response to volcanic forcing in the 20th century has been ascribed as one of the potential causes of the Sahel drought and the weak West African monsoon of the 1970s–1990s [10, 16].

However, Sahelian rainfall and, more in general, tropical precipitation are strongly tied to sea surface temperature (SST [17, 18]). Year-to-year monsoon

variability depends in fact on diverse drivers, mainly related to large-scale patterns of SST and sea level pressure of adjacent oceans: the Atlantic Multidecadal Variability, Indian Ocean Dipole and Indo-Pacific Warm Pool have been teleconnected with Indian, African and Australian monsoons (e.g. [19]), the Pacific Decadal Oscillation impacts more the North American sector, while El-Niño Southern Oscillation (ENSO) affects preferentially Indian, Australian and South American monsoons [20–24]. All these observable patterns or modes of climate variability result from heat and moisture exchanges within the climate system, and are often identified as internal climate variability.

Given the superposition of the volcanic forcing and internal climate variability on monsoon dynamics at interannual time scale, disentangling the effect of two sources of natural forcing for attribution studies is difficult and deserves a well-designed climate model experiment. For this purpose, large ensembles that facilitate separation of the volcanic forced response from internal variability are needed, as well as sophisticated statistical analysis methods [25, 26]. Earth System Model Large Ensembles provides an excellent database to understand the interactions between forced and unforced variability [27–29]. The advantage is to explore the sensitivity of global and regional monsoons to volcanic eruptions beyond the range of the internal climate variability. This approach has important implications for the predictability of monsoons. Zuo *et al* [3] attributed the response of global and regional monsoons to volcanic eruption within the Large Ensemble framework, by using the CESM-LM ensemble [30]. This dataset covers the last millennium (850-2005 CE) and the forcing to drive the model uses version 1 of the Gao *et al* reconstructions based on volcanic deposition signals from Arctic and Antarctic ice-core records [31]. However, one difficulty in evaluating the historical and last millennium ensembles is that the volcanic eruptions differ not only in their strength but also in the geographical latitude and season of the eruption, which means that it is not possible to draw direct conclusions about the dependence of monsoons on the emission strength of the eruption.

Our approach is different from previous studies, as it is based on an experiment encompassing 100-member ensembles for five idealized equatorial volcanic eruptions of different strengths [32], which are branched off in January 1991 from the historical Max Planck Institute Earth System Model Grand Ensemble (MPI-GE [27]) and ran for a 3-year period. This experiment allows us to explore the full range of monsoon sensitivity to 'Pinatubo-like' volcanic eruptions of different strengths and to pose new questions: is the monsoonal precipitation response linear to the strength of the eruption? Does an emission threshold exist for getting a robust response? Are regional monsoons equally vulnerable to equatorial volcanic eruptions?

2. Data and methods

2.1. The MPI-GE EVA ensemble

The climate system is modulated by internal variability and external forcing [33]. However, the climate response to external forcing can be separated from internal climate variability with large ensembles [29]. In this study we use the historical simulations of one of the largest ensembles currently available: the Max Planck Institute Earth System Model Grand Ensemble (MPI-GE [27]), which encompasses a 100-members ensemble of several CMIP5 experiments. The MPI-GE is based on the low-resolution version of the Max-Planck-Institute Earth-System-Model (MPI-ESM1.1-LR), a further developed version of the MPI-ESM CMIP5 version [34], which couples the atmospheric general circulation model ECHAM6.3 in its T63 configuration and 47 vertical levels up to 0.01 hPa [35], with the ocean-sea ice model MPIOM in its GR15 configuration with 64 vertical levels [36]. JSBACH3.0 [37] represents the land, and HAMOCC5.2 [38] the ocean biogeochemistry component of the MPI-ESM. Further details on the model and the MPI-GE are given in Maher *et al* [27].

The volcanic aerosol forcing in MPI-ESM is prescribed by monthly zonal mean wavelength dependent optical properties which are interpolated linearly in time for the radiative transfer calculations. In the MPI-GE historical simulations an extended version of the Pinatubo aerosol dataset was used, as for CMIP5 historical simulations [39, 40]. The historical MPI-GE experiment is able to capture the co-occurrence of El-Niño events and major volcanic eruptions, as well as the co-variance between Northern/SH volcanic forcing and El-Niño/La Niña phases [41].

Within the MPI-GE historical framework, we use an additional set of sensitivity experiments designed for disentangling the impact of volcanic forcing from the internal variability, the Easy Volcanic Aerosol ensemble (EVA ensemble) [32]. In EVA ensemble, the Mt. Pinatubo volcanic forcing in the MPI-GE historical simulations has been replaced by monthly and zonal mean forcing fields of idealized tropical eruptions which have been compiled with the EVA forcing generator [42]. All other forcings remained fixed. EVA provides a simplified representation of volcanic stratospheric aerosol forcing, prescribing aerosol extinction, single scattering albedo and asymmetry factor and their space-time structure as a function of sulfur emission strength, eruption location and season and wavelength.

We consider five idealized Pinatubo-like equatorial June eruptions with different eruption strengths:

2.5, 5, 10, 20 and 40 $\times 10^{12}$ g of sulfur (Tg S). The estimated June 1991 Pinatubo eruption sulfur emission is within 5–10 Tg S range [32]. In addition, a run without volcanic forcing has been performed (EVA0, 0 Tg S).

All of the different EVA ensembles contain 100 ensemble members and have been initialized from one of the 100 members of the MPI-GE historical ensemble in January 1991. Figure SI1 (available online at stacks.iop.org/ERL/17/054001/mmedia) shows the prescribed stratospheric aerosol optical depth (SAOD) at 0.55 μm for the five idealized equatorial eruptions and the corresponding CMIP5 forcing for the Pinatubo episode originally used in the historical MPI-GE. In general, all the EVA ensembles' forcing data show a similar SAOD pattern, albeit of different magnitude with a tropical maximum for the 1st months after the eruption and a transport to NH mid-to-high latitude with the seasonal change to NH winter circulation. In comparison to the CMIP5 dataset, the EVA ensemble show less aerosol in the extratropics compared to the tropics. In the idealized simulations the aerosol moves faster to the NH extratropics and also disappears faster. In the SH extratropics the CMIP5 historical Pinatubo dataset shows more aerosol, as it is based on satellite observations and therefore also includes the historic eruption of Cerro Hudson (45° S) in August 1991.

In the following we will use the term EVA X to characterize the MPI-ESM 100-member ensemble of an idealized volcanic eruption with an emission strength of X Tg S.

We compare our EVA ensemble results with monthly ERA-20C reanalysis and Global Precipitation Climatology Project (GPCP) for years 1988–1992, before and after the Pinatubo eruption. ERA-20C is a deterministic reanalysis [43] meant to reproduce the actual weather evolution and the observed occurrence of synoptic systems, the low frequency variability and mean state of the atmosphere in the 20th century. The atmospheric model is the IFS at the T163 spectral horizontal resolution forced with CMIP5 prescription of the historical simulation. Moreover, the atmospheric model of ERA-20C uses prescribed HadISST2.1 and assimilates marine surface winds and surface and mean sea level pressure. Given its configuration, ERA-20C describes realistic long-term evolution of the 20th century climate, including the occurrence of major events, such as ENSO and major volcanic eruptions, being therefore perfectly suited for comparing MPI-GE model results. GPCP dataset results from rain gauge stations, satellites, and sounding observations merged on a 2.5-degree global grid from 1979 to the present [44]. The careful combination of satellite-based rainfall estimates provides the most complete analysis of rainfall available to date over the global oceans, and adds necessary spatial detail to the rainfall analyses over land. The dataset is commonly used for climate model validation of global precipitation, as they use comparable grids. The current version is GPCPv2.3, which does not include the precipitation estimates from TRMM, GPM, or Cloudsat, therefore the global-mean precipitation amount is underestimated, possibly due to missing light rain over ocean and orographic precipitation over land.

2.2. Analysis tools

2.2.1. Monsoon statistics

Global monsoon area and intensity are assessed using the definition of global monsoon by Wang *et al* [45], i.e. where local summer-minus-winter precipitation rate exceeds 2 mm d^{-1} and the local summer precipitation exceeds 55% of the annual total. Local summer is May through September (MJJAS) for the NH and November through March (NDJFM) for the SH. The selected threshold allows us to distinguish the monsoon regime area from the adjacent dry regions where the local summer precipitation is less than 1 mm d^{-1}, and equatorial climate region. Once the global monsoon domain has been identified for each year of the simulation, we have computed its size (monsoon area). The monsoon intensity is the area-average precipitation in JJA for NH and in DJF for SH within the global monsoon, its ocean and land parts, and of each continental sub-region: North America, North Africa and South East Asia (NAM, NAF, SAS) in the NH, South America, South Africa and Australia (SAM, SAF, AUS) in the SH. It is worth noting that for the SH monsoons, December 1991 belongs to 'First Year' and December 1992 to 'Second Year' after the volcanic eruption of that year's DJF season.

2.2.2. Local Hadley and Walker circulations

The tropical atmospheric vertical flow in pressure coordinates has been decomposed following Schwendike *et al* [46] and Nguyen *et al* [47] into zonal and meridional overturning, defining the Walker and local-Hadley circulations, respectively. D'Agostino *et al* [8] showed that for each monsoon domain it is possible to identify a regional meridional overturning, given the strong relationship between the cross-equatorial Hadley circulation and monsoons [48]. Horizontal winds are first decomposed into rotational and divergent components in spherical coordinates, where only the latter part contributes to the vertical motion. Then, the divergent component of the meridional flow, related to Hadley circulation and the divergent component of the zonal flow between 5° S and 5° N, related to Walker circulation have been vertically integrated in the tropospheric layer (see local stream function in [49] and appendix in D'Agostino *et al* [8]). This mass-conserving method ensures the decomposition of the divergent motion into two unique orthogonal overturning circulations that are the sum of the total divergent flow.

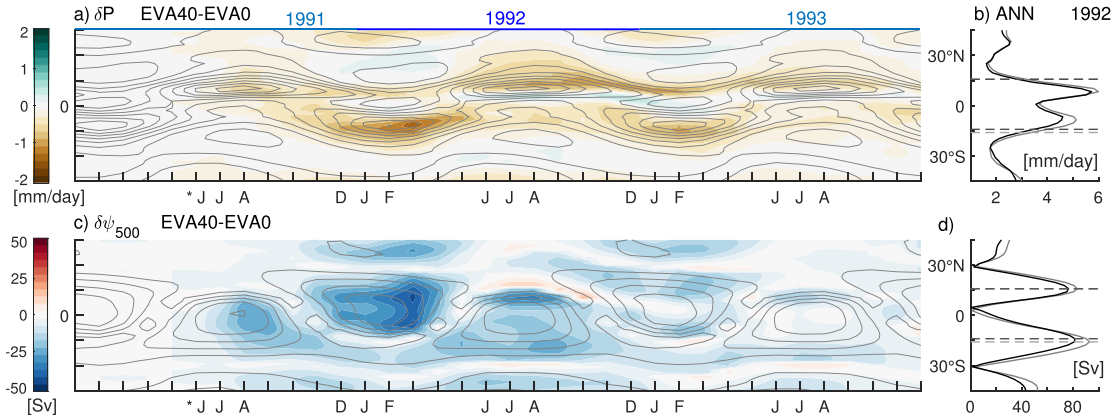

Figure 1. Time-latitude plots of zonal mean precipitation (panel (a), mm d^{-1}) and stream function at 500 hPa (panel (c), Sverdrups [Sv] $= 10^9$ kg s^{-1}) difference between EVA40 and EVA0 ensemble means (shaded colors). Grey contour lines are EVA0. Note that in panels (c) and (d) the stream function is defined positive for both, Northern and SH, so that the anomalies relative to the control have unambiguous signs (see panel (d)). Annual (December 1991–November 1992) and zonal mean precipitation (panel (b)) and stream function at 500 hPa (panel (d)) for EVA40 (black line) and EVA0 (grey lines) for the year 1992. Horizontal dashed lines in panels (b) and (d) indicate the width of the ITCZ aka the rain belt, i.e. the latitudinal distance between the minimum and maximum of the stream function in the Southern and NH, respectively [51].

3. Results

3.1. Zonal mean tropical precipitation and atmospheric overturning

The effect of equatorial volcanic eruptions on tropical hydroclimate lasts for some years after the event, regardless of the strength of forcing (figures 1, SI2 and SI3). In particular, the strongest impact takes place from a couple of months after the eruption (June 1991) until the end of 1992 boreal summer, a period that encloses the summer monsoon season in the SH (December 1991–February 1992) and in the NH (June–August 1992). The difference between the experiment with the strongest forcing (40 Tg S, EVA40) and EVA0 supports decreased overall tropical precipitation, especially at the southern flank of the rain belt, which leads to a narrower ITCZ (figure 1). Precipitation anomalies are particularly strong in the summer months of the respective hemisphere (DJF for SH and JJA for NH). Figure 1(c) shows the time evolution of 500 hPa anomalous zonal mean meridional mass streamfunction (color shades) against the control (contours). For simplicity, the stream function has been kept positive at each latitude (y-axis, figures 1(c) and (d)), so the colored anomalies are easier to interpret. The decreased tropical precipitation shown in figure 1(a) is supported by the correspondent weakening of the cross-equatorial Hadley circulation (i.e. the one in the opposite hemisphere) and narrowing of its upward branch between 1991 and 1992 (figures 1(c) and (d)).

3.2. Global and regional monsoons

Considering the time period of the strongest impact (December 1991–August 1992), the summer precipitation in the global monsoon domain declines in both hemispheres with increasing emissions (figures 2 and SI2), especially over land (figures 2 and 3). In particular, only a stronger than Pinatubo-like eruption (Tg S $\geqslant$ 10) significantly affects the monsoon intensity, with boxes of figure 3 being outside the range of EVA0 without volcanic forcing (representing the internal variability in the model). Conversely, the area of the global monsoon is less affected: it is narrower for EVA40 but the change is generally within the range of the internal variability for every experiment (figure 3).

As the stratospheric volcanic aerosols reflect sunlight, the evaporation is reduced, whilst surface cooling stabilizes the atmosphere and reduces its water-holding capacity. This leads to pronounced circulation changes, which modulate the global precipitation reduction on regional scales, with altered dry-wet patterns (figure 2): dry regions become wetter while wet regions become drier. The deviation from the global drying pattern suggests a modification of the overturning circulation in the meridional sense (Hadley-Ferrel circulations), with important regional hydroclimate impacts.

In fact, volcanic eruptions have a strong regional fingerprint (figure 2). Precipitation anomalies are largely zonally asymmetric despite the equatorial zonally-symmetric volcanic forcing. NAF, SAS, SAF and SAM precipitation are the most sensitive to equatorial volcanic forcing (figure 3). In these regions, the precipitation declines for emissions ranging the full spectrum of the experiments. On the other hand, the regional monsoon area does not change significantly for most of the considered domains, except a slight contraction for the ocean part and for SAF and NAM in the case of EVA40.

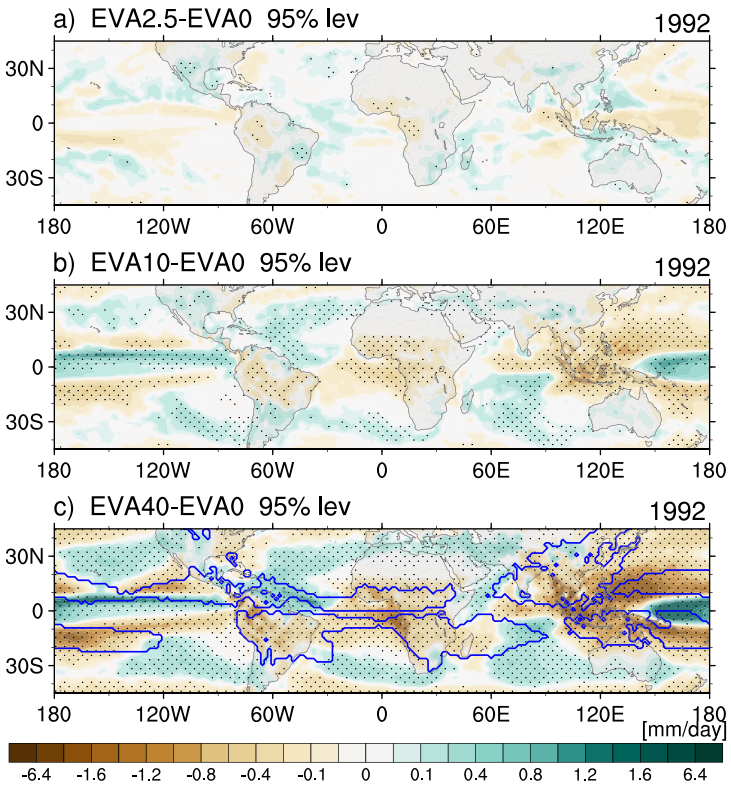

Figure 2. Composite summer precipitation difference (mm d^{-1}) between EVA2.5, EVA10, EVA40 and EVA0. The panels show at the same time the NH summer (0–45° N, JJA 1992) and SH summer (0–45° S, DJF 1991/1992) of the first year after the volcanic eruption. Dots represent 95% confidence level. The blue contour is the global monsoon domain in EVA40.

3.3. Atmospheric overturning changes: Hadley and Walker circulations

The Hadley circulation is usually described by the stream function in the meridional plane, with upwelling at the deep tropics (where the moist air converges in the low levels and uplifts generating the ITCZ) and downwelling at subtropics. The effect of volcanic forcing has important implications on the overall structure of the zonal mean overturning (figure 1, and ZM in figures 4 and 5): the cross-equatorial zonal mean Hadley circulation (i.e. the one associated with monsoons in the opposite hemisphere) weakens and shrinks immediately after the eruption and for the successive years (1991/1992, figures 1, SI3). Additionally, the position of the upwelling shifts towards the equator, the ITCZ is narrower (figure 1, panels (b) and (d)) and the circulation is shallower (as shown by stronger anomalies on the top levels of the stream function associated with a tropopause height decrease, figures 4 and 5).

Regionally, in the NH, SAS and NAF are the two sectors showing the largest anomalies (figure 4). In the SH, SAF and SAM are the sectors more affected than the others by the volcanic forcing with the respective cross-equatorial Hadley circulation being weaker (figure 5). The sole exception to the overall weakening of tropical circulation is represented by the stronger Hadley circulation in the Australian-Maritime Continent sector. Overall, the weakening and shrinking of the local Hadley circulation is consistent with the simulated rainfall decline in the respective monsoon regions (figure SI3), global dry-wet patterns (figure 2) and with decreased NEI at the ITCZ (figure SI4). Also the Walker circulation (similarly described by the stream function in the zonal plane) is weaker and shifted eastward in the DJF 1992 (figure 5).

3.4. The relative influence between net energy input and gross moist stability on tropical overturning weakening

Can we relate the weakening of overturning under volcanic forcing and the decreased precipitation just to changes in the atmospheric net energy input (NEI)?

Following the energetic framework, in a steady state and assuming that eddy fluxes are small, the export of moist static energy (MSE) by the Hadley circulation is balanced by the NEI at the ascent. Neelin and Held, [50] showed that, to first order, the export of MSE by the Hadley circulation is given by the product of the gross moist stability (GMS, a measure of the tropospheric MSE stratification at ITCZ) and the strength of the Hadley circulation's ascent.

Under climate change (for whatever the reason, e.g. CO_2, aerosols, volcanic forcing, etc), a change in NEI must be associated with a change in MSE export, which is itself achieved by changes in GMS and/or in

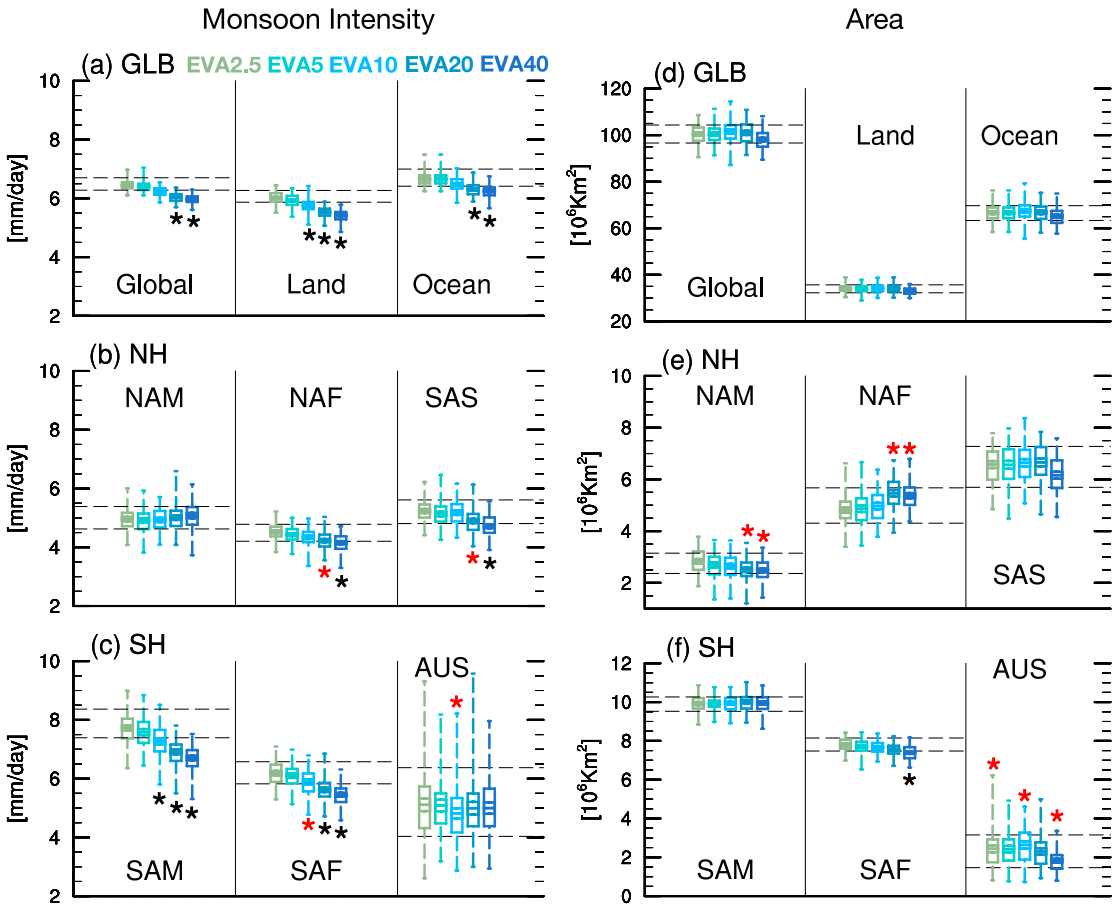

Figure 3. Global monsoon intensity (left, mm d^{-1}) and area (right, 10^6 km^2) computed for the first year after the volcanic eruption (1992). Global monsoon (top row, GLB, panel (a) and (d)) is computed according to the definition by Wang *et al* [45], for different volcanic eruption strengths (*x*-axis, colored box-and-whiskers, 2.5, 5, 10, 20, 40 Tg (S). Land and ocean parts (a), (d) are computed by applying the land/ocean mask to the global monsoon precipitation. On the other hand, regional monsoons are selected values of land monsoons in their respective domains: North America (NAM: [0, 30° N; 120° W, 40° W]), North Africa (NAF: [0, 30° N; 20° W, 40° E]), South Asia (SAS: [0, 30° N; 70° E, 120° E]), South America (SAM: [0, 30° S; 90° W, 30° W]), South Africa (SAF: [0, 30° S; 0, 60° E]), Australia (AUS: [0, 30° S; 90° E, 170° E]). Grey dashed lines indicate the mean ±2 standard deviation of EVA0. Boxes-and-whiskers show the mean, the 95% confidence interval, the 25th and 75th percentiles, and extremes. Red asterisks indicate substantial changes, when the ensemble mean of (EVA X—EVA0)/EVA0 exceeds 5%. Substantial and statistically significant results are shown by a black asterisk.

the strength of the Hadley circulation upwelling: for a negative NEI anomaly the circulation weakens; for a positive input, it strengthens. However, the effect of moisture on the overturning strength is fundamentally important as well. In fact, assuming that the NEI does not change in a target experiment relative to its control, the circulation has to weaken when the convergence of humidity increases at its low levels (e.g. under global warming circumstances).

Here we test the energetic framework and we check the relative influence between NEI and GMS in weakening the ascent of tropical overturning in EVA40 and EVA0 (see the definition of ascent by Byrne *et al* [51] and dashed lines in figure 1). Chou *et al* [52], for example, have used a similar approach in global warming experiments by plotting changes in GMS against changes in ascent.

In our EVA40 experiment, the slope of the linear fit between the NEI (*x*-axes) and integrated upwelling (*y*-axes) among the 33-month EVA simulations (filled dots, figure 6), excluding the 3-months right after the eruption (July–September 1991, open dots) is 2. The deviation from the 1:1 line, the perfect case in which the relative reduction of NEI aligns with the relative weakening of the overturning, means that the reduction of the MSE export and the weakening of the atmospheric circulation under volcanic forcing can be explained by a comparable NEI reduction and GMS increase at the ITCZ. The increased GMS under volcanic forcing results from increased MSE at the top-of-troposphere as a consequence of stratospheric warming (figure SI5 and [53]).

4. Discussions and conclusions

The effect of volcanic forcing on tropical circulation has been well documented in the last millennium

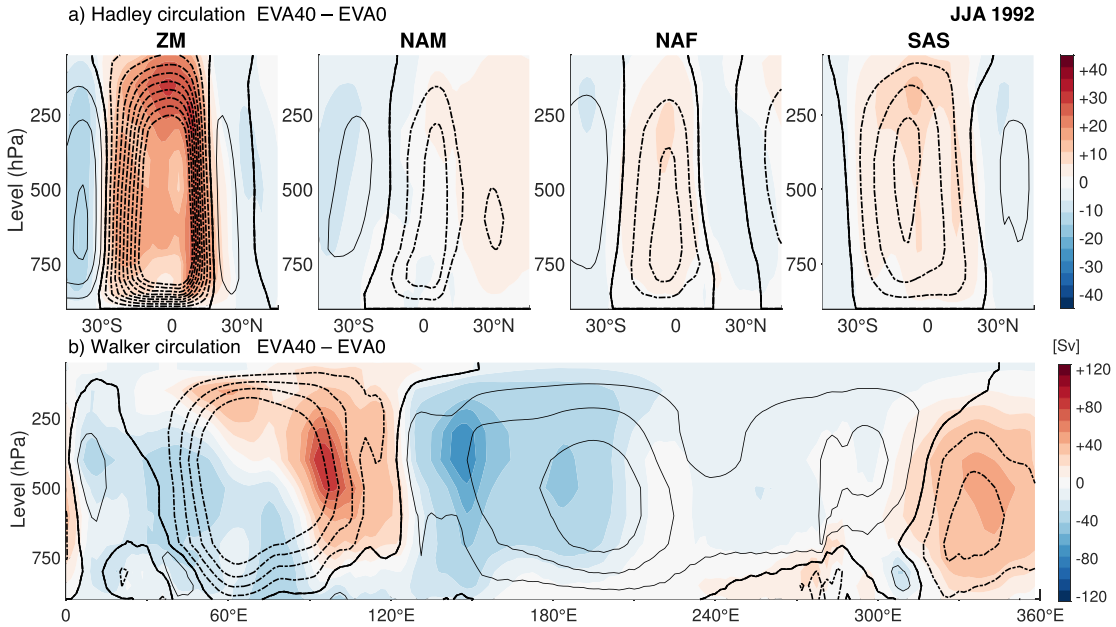

Figure 4. Ensemble mean difference of stream function between EVA40 and EVA0 in JJA 1992. Top panel shows the local Hadley cells computed in each monsoon domain—ZM, NAF, SAS, NAM, Zonal mean, North Africa, South Asia and North America respectively. Bottom panel shows the Walker cell computed between 5° N and 5° S. Colors show the anomalous circulation relative to EVA0. Contours refer to EVA0 (contour step is 1×10^9 kg s^{-1}). Solid (dotted) lines indicate positive (negative) values of the stream function for clockwise (counterclockwise) circulation.

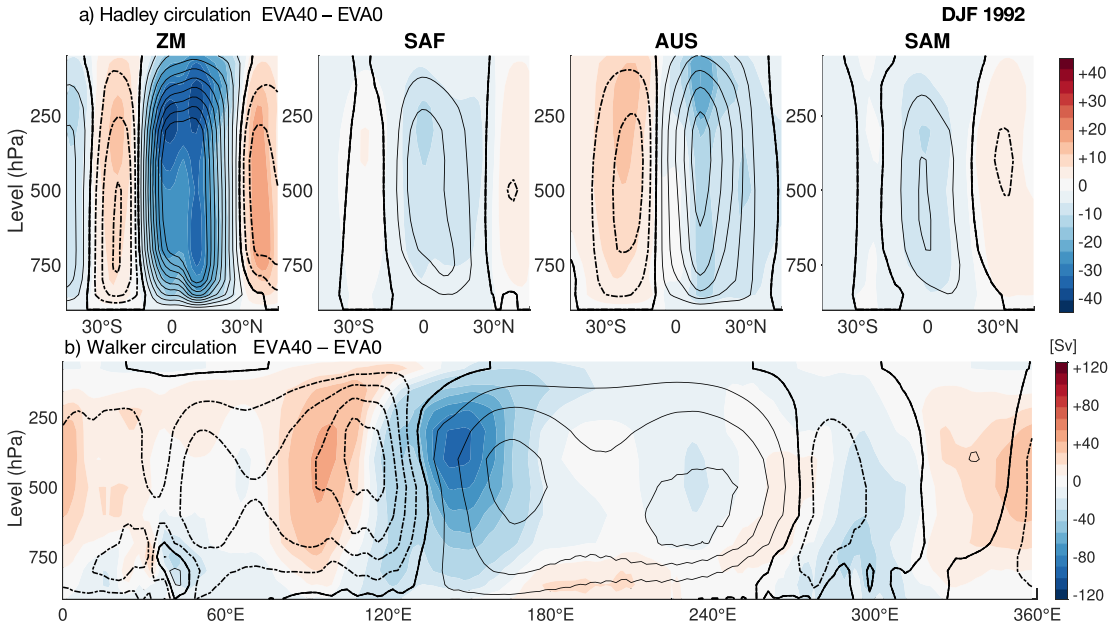

Figure 5. Ensemble mean difference of stream function between EVA40 and EVA0 in DJF 1991/1992. Top panel shows the local Hadley cells computed in each monsoon domain—ZM, SAF, AUS, SAM, Zonal mean, South Africa, Australia and South America respectively. Bottom panel shows the Walker cell computed between 5° N and 5° S. Colors show the anomalous circulation relative to EVA0. Contours refer to EVA0 (contour step is 1×10^9 kg s^{-1}). Solid lines indicate positive values of the stream function for clockwise circulation, while dotted lines indicate negative values and counterclockwise circulation.

proxy reconstructions and simulations (e.g. [3] and references therein). However, while previous work has highlighted the importance of asymmetric volcanic forcing (e.g. [10, 15, 41, 54]), our study points for the first time the potential impact of a wide range of tropical symmetric volcanic eruptions on tropical circulation and monsoon precipitation beyond the influence of the internal variability. By using a 100-member large ensemble of five idealized equatorial volcanic eruptions with different sulfur emission strengths between 2.5 to 40 Tg S, we have narrowed the uncertainties in the results of previous studies, which are either based on super-epoch analysis of different magnitude, or based on volcanic eruptions over

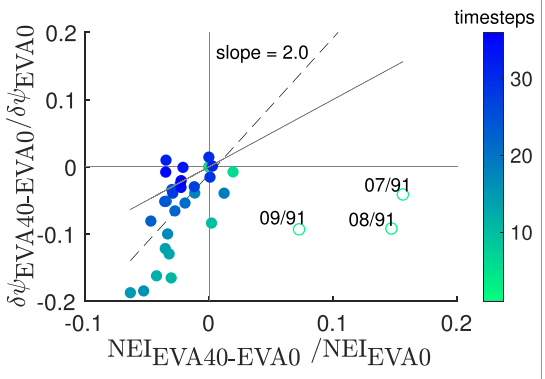

Figure 6. Scatterplot (dashed black line) of ensemble mean values of anomalous atmospheric NEI ($NEI_{EVA40-EVA0}$) versus anomalous integrated tropical upwelling ($\psi_{max} - \psi_{min} = \delta\psi$ difference between EVA40 and EVA0) normalised by EVA0 and evaluated at the ITCZ (figure 1 in Byrne and Schneider, 2018). Colored dots show the months of the simulation (1 to 36 from green to blue). The linear fit accounts only for filled dots, while open dots from the initial phase, i.e. the 3 months right after volcanic eruption are neglected.

the common era with varying sulfur emission and/or eruption latitudes and/or seasons (e.g. [3, 55, 56]), or based on a smaller ensemble size (10–20 members) for specific eruptions (e.g. [56, 57]).

The equatorial volcanic forcing shapes the global hydroclimate, with altered dry-wet patterns: under volcanic forcing wet regions become drier and dry regions, such as Mediterranean and mid-latitudes, become wetter than the unperturbed climate [58, 59]. Following the altered dry-wet patterns and the land/ocean energy contrasts, land monsoon intensity is preferentially affected by volcanic eruptions and results in weaker monsoons, while the extent of the global and regional monsoon does not change significantly. In particular, only a stronger or Pinatubo-like eruption ($\geqslant$10 Tg S) can significantly affect the monsoonal precipitation beyond the effect of internal variability and at least for two years after the events (Figures 3, SI2). Furthermore, the symmetrical forcing with an idealised equatorial eruption results in zonally asymmetric anomalous precipitation, with regional heterogeneity among the monsoon domains: African and Australasian sectors are more sensitive to the forcing given the correspondent regional Hadley and Walker overturning shifts. Zuo *et al* [3] found dynamic processes related to changes in atmospheric circulation playing a dominant role in precipitation responses. They suggested that for tropical eruptions, the reduction in monsoon precipitation is a result of a decreased land-ocean thermal contrast and an anomalous warming in the eastern Pacific. Our study agrees with previous findings on monsoon precipitation response to last millennium tropical volcanic eruptions [3, 60].

During the last millennium and the 20th century, large volcanic eruptions were often simultaneous to El-Niño events [3, 41, 60]. Given the superposition of Pinatubo-1991 volcanic eruption and El-Niño, which is also known for its large impact on monsoon systems, we have explored their relative influence on tropical precipitation in the ensemble space. In our simulations, the Oceanic Niño Index (i.e. the relative SST anomalies in the El-Niño 3.4 region, see supplementary for its computation following Khodri *et al* [61]) shows a moderate El-Niño event during the summer 1992 in EVA40 (figure SI6(a)) in agreement with previous studies who have found an El-Niño like response to volcanic forcing after large tropical eruptions (e.g. [61–63]). Then, it is questionable if the overall precipitation response in our experiments is due to the effect of volcanic forcing or to the El-Niño. Both in fact weaken the Australasian monsoons, where the Walker circulation teleconnects Indian and Pacific SSTs (e.g. [20, 62–64]). We tested if the two responses are different for the case of the strongest sulfur emission (figure SI6). The response of JJA 1992 precipitation is substantially different between El-Niño and volcanic forcing in EVA40 (figures SI6(b)–(d)). In fact, considering EVA0, the El-Niño in the unperturbed simulation has a slight drying effect on land monsoon precipitation in the NH (figure SI6(b)). On the other hand, El-Niño events in the perturbed simulations with the strongest volcanic eruption EVA40 increases the overall land monsoon rainfall (figure SI6(c)): this result highlights the nonlinear response of precipitation to the combination of both forcings (figure SI6(e)). As shown by other studies, El-Niño tends to shift the ITCZ southward and the position of Walker circulation's main updraft eastward. Conversely, the volcanic forcing has a prevalent drying effect in South-East Asian and Australian sectors and over lands. From our analysis it seems that El-Niño modulates slightly the hydroclimate response to strong volcanic forcing. Our results with the EVA ensemble show that it is possible to disentangle the two effects on tropical hydroclimate, and they result in very different precipitation patterns, if the volcanic forcing is strong enough.

A comparison of our model results with observations is difficult as we consider idealized equatorial eruptions. We know from the literature that the multimodel mean of CMIP5 models fails to reproduce the observed magnitude of rainfall anomalies over some monsoon domains [5, 6, 65–67] and CMIP6 models do not perform better tropical precipitation relative to previous CMIP generations [68]. Additionally, simulated post-volcanic changes of the monsoon systems significantly deviate from paleo-records [69]. Nevertheless there is some qualitative agreement with proxy reconstructions at least on the sign of the change, i.e. tropical belt contracts and monsoonal precipitation decreases for some years after the volcanic eruptions [41, 56, 70].

Our idealized experiments confirm the dynamically-induced decreased monsoon precipitation and show that a sulfur emission $\geqslant$10 Tg S,

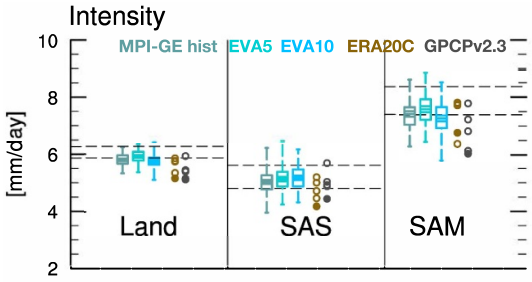

Figure 7. Monsoon intensity (mm d^{-1}) computed for the first year after the volcanic eruption (1992) for Land, Indian (SAS) and South American (SAM) monsoons. Grey dashed lines indicate the mean ±2 standard deviation of EVA0. Boxes-and-whiskers show the mean, the 95% confidence interval, the 25th and 75th percentiles, and extremes for MPI-GE historical, EVA5 and EVA10 simulations. Dots indicate ERA-20C reanalysis (brown) and GPCPv2.3 (grey): open dots for years 1988, 1989, 1990 and 1991, and closed dots for year 1992. Both datasets have been interpolated on the same horizontal grid of MPI-GE.

which is the upper estimate of the June1992 Pinatubo eruption, could be considered as a threshold value to obtain a significant tropical hydroclimate response, as indicated by the distribution of ensemble members of both EVA10 and MPI-GE against the internal variability of the EVA0 (figure 7). For the most sensitive land monsoons, our results show that, despite the wet bias of the ensemble mean of the unperturbed run (EVA0) relative to observations, the JJA 1992 monsoon precipitation (land, SAS and SAM) of GPCP data and ERA-20C reanalysis fall within the lower extremes of MPI-GE and EVA5 and EVA10 ensemble members (filled brown and gray dots for JJA 1992 in figure 7). However, while GPCP data and ERA-20C indicate for all regions a decrease in precipitation in 1992, the model shows a slight increase in precipitation for SAS and only a decrease for the much stronger eruption (EVA40).

While we have focused only on the monsoon sensitivity to the eruption magnitude, other factors might be important as well for understanding the complex precipitation response to volcanic forcing: the overall response will certainly be altered if we consider volcanic eruptions with different hemispherically asymmetric forcing, but also oceanic initial conditions could lead to regional differences in the tropical SST response (e.g. [56, 57, 63]). The relative role of initial conditions and radiative forcing to the tropical precipitation response might be conditioned depending on the magnitude of the forcing. In the case of a large eruption, the direct radiative forcing dominates, as shown here for the idealized tropical 40 Tg S eruption. However, this aspect will be addressed in detail in a separate study.

While large initial condition ensembles, such as the EVA ensemble, are well suited to disentangle the forced response from internal variability, the results are model dependent. Paik *et al* [63] found a large inter-simulation spread in the hydrologic responses to tropical volcanic eruptions in 35 CMIP5 models. However, first insights from the VolMIP multimodel intercomparison show a general inter-model agreement for the idealized Pinatubo experiment despite uncertainties in the radiative flux response and dependence on sampled initial states [71] Similar experiments like the EVA ensemble for idealized tropical but also for NH/SH eruptions in a multimodel framework such as CMIP6/VolMIP [72] would therefore be desirable for the future.

Data availability statement

The data that support the findings of this study are available upon reasonable request from the authors.

Acknowledgments

Authors acknowledge Juergen Bader for his comments on the draft, Renate Brokopf for her help with NCL scripts for producing figures 2 and 3, Alon Azoulay and Hauke Schmidt for providing the EVA ensemble model output and David Ferreira for the inspiring conversations about the relationship between the net energy input and the tropical overturning strength.

Roberta D'Agostino is funded by the Deutsche Forschungsgemeinschaft (DFG, German Research Foundation) under Germany's Excellence Strategy-EXC 2037 Climate, Climatic Change, and Society (CLICCS)-Cluster of Excellence Hamburg, A4 African and Asian Monsoon Margins, Project Number: 390683824.

Claudia Timmreck is funded by the DFG research unit FOR 2820: Revisiting The Volcanic Impact on Atmosphere and Climate-Preparations for the Next Big Volcanic Eruption (VolImpact, Project Number: 398006378).

ORCID iDs

Roberta D'Agostino https://orcid.org/0000-0002-0717-6186
Claudia Timmreck https://orcid.org/0000-0001-5355-0426

References

[1] Robock A 2000 *Rev. Geophys.* **38** 191–219
[2] Timmreck C, Graf H F, Zanchettin D, Hagemann S, Kleinen T and Krüger K 2012 *Quat. Int.* **258** 30–44
[3] Zuo M, Zhou T and Man W 2019 *J. Clim.* **32** 4367–85
[4] Held I M and Soden B J 2006 *J. Clim.* **19** 5686–99
[5] Iles C E and Hegerl G C 2014 *Environ. Res. Lett.* **9** 104012
[6] Iles C E and Hegerl G C 2015 *Nat. Geosci.* **8** 838–42
[7] D'Agostino R, Bader J, Bordoni S, Ferreira D and Jungclaus J 2019 *Geophys. Res. Lett.* **46** 1591–601
[8] D'Agostino R, Brown J R, Moise A, Nguyen H, Silva Dias P L and Jungclaus J 2020 *J. Clim.* **33** 9595–9613
[9] Oman L, Robock A, Stenchikov G L and Thordarson T 2006 *Geophys. Res. Lett.* **33**
[10] Haywood J M, Jones A, Bellouin N and Stephenson D 2013 *Nat. Clim. Change* **3** 660–5
[11] Pausata F S R, Grini A, Caballero R, Hannachi A and Seland Ø 2015 *Tellus* B **67** 26728
[12] Pausata F S, Chafik L, Caballero R and Battisti D S 2015 *Proc. Natl Acad. Sci.* **112** 13784–8
[13] Pausata F S R, Karamperidou C, Caballero R and Battisti D S 2016 *Geophys. Res. Lett.* **43** 8694–702
[14] Ridley H E *et al* 2015 *Nat. Geosci.* **8** 195–200
[15] Jacobson T W, Yang W, Vecchi G A and Horowitz L W 2020 *Clim. Dyn.* **55** 1733–58
[16] Herman R J, Giannini A, Biasutti M and Kushnir Y 2020 *Sci. Rep.* **10** 1–11
[17] Mohino E, Janicot S and Bader J 2011 *Clim. Dyn.* **37** 419–40
[18] Good P, Chadwick R, Holloway C E, Kennedy J, Lowe J A, Roehrig R and Rushley S S 2021 *Nature* **589** 408–14
[19] Monerie P A, Robson J, Dong B, Hodson D L and Klingaman N P 2019 *Geophys. Res. Lett.* **46** 1765–75
[20] Webster P J and Yang S 1992 *Q. J. R. Meteorol. Soc.* **118** 877–926
[21] Ambrizzi T, de Souza E B and Pulwarty R S 2004 The hadley and walker regional circulations and associated enso impacts on south american seasonal rainfall *The Hadley Circulation: Present, Past and Future* (Berlin: Springer) pp 203–35
[22] Turner A G and Slingo J M 2011 *Clim. Dyn.* **36** 1717–35
[23] Jourdain N C, Gupta A S, Taschetto A S, Ummenhofer C C, Moise A F and Ashok K 2013 *Clim. Dyn.* **3** 660–5
[24] Kucharski F and Abid M A 2017 Interannual variability of the Indian monsoon and its link to Enso *Oxford Research Encyclopedia of Climate Science*
[25] Bittner M, Schmidt H, Timmreck C and Sienz F 2016 *Geophys. Res. Lett.* **43** 9324–32
[26] Pauling A G, Bushuk M and Bitz C M 2021 *Geophys. Res. Lett.* **48** e2021GL092558
[27] Maher N *et al* 2019 *J. Adv. Model. Earth Syst.* **11** 2050–69
[28] Deser C *et al* 2020 *Nat. Clim. Change* **10** 277–86
[29] Milinski S, Maher N and Olonscheck D 2020 *Earth Syst. Dyn.* **11** 885–901
[30] Otto-Bliesner B L, Brady E C, Fasullo J, Jahn A, Landrum L, Stevenson S, Rosenbloom N, Mai A and Strand G 2016 *Bull. Am. Meteorol. Soc.* **97** 735–54
[31] Gao C, Robock A and Ammann C 2012 *J. Geophys. Res.* **117** D16112
[32] Azoulay A, Schmidt H and Timmreck C 2021 *J. Geophys. Res.* **126** e2020JD034450
[33] Suarez-Gutierrez L, Maher N and Milinski S 2020 *US CLIVAR Variations* **18** 27–35
[34] Giorgetta M *et al* 2013 *J. Adv. Model. Earth Syst.* **5** 572–97
[35] Stevens B *et al* 2013 *J. Adv. Model. Earth Syst.* **5** 146–72
[36] Jungclaus J, Fischer N, Haak H, Lohmann K, Marotzke J, Matei D, Mikolajewicz U, Notz D and Storch J 2013 *J. Adv. Model. Earth Syst.* **5** 422–46
[37] Reick C H, Raddatz T, Brovkin V and Gayler V 2013 *J. Adv. Model. Earth Syst.* **5** 459–82
[38] Ilyina T, Six K D, Segschneider J, Maier-Reimer E, Li H and Nú nez-Riboni I 2013 *J. Adv. Model. Earth Syst.* **5** 287–315
[39] Stenchikov G L, Kirchner I, Robock A, Graf H-F, Antuña J C, Grainger R G, Lambert A and Thomason L 1998 *J. Geophys. Res.* **103** 13837–57
[40] Schmidt H *et al* 2013 *J. Adv. Model. Earth Syst.* **5** 98–116
[41] Ward B, Pausata F S R and Maher N 2021 *Earth Syst. Dyn.* **12** 975–96
[42] Toohey M, Stevens B, Schmidt H and Timmreck C 2016 *Geosci. Model Dev.* **9** 4049–70
[43] Poli P *et al* 2016 *J. Clim.* **29** 4083–97
[44] Adler R *et al* 2016 *Natl Centers Environ. Inf.* **10** V56971M6
[45] Wang B, Liu J, Kim H J, Webster P J, Yim S Y and Xiang B 2013 *Proc. Natl Acad. Sci.* **110** 5347–52
[46] Schwendike J, Berry G J, Reeder M J, Jakob C, Govekar P and Wardle R 2015 *J. Geophys. Res.* **120** 7599–618
[47] Nguyen H, Hendon H, Lim E P, Boschat G, Maloney E and Timbal B 2018 *Clim. Dyn.* **50** 129–42
[48] Bordoni S and Schneider T 2008 *Nat. Geosci.* **1** 515–9
[49] D'Agostino R, Scambiati A L, Jungclaus J and Lionello P 2020 *Geophys. Res. Lett.* **47** e2020GL089325
[50] Neelin J D and Held I M 1987 *Mon. Weather Rev.* **115** 3–12
[51] Byrne M P, Pendergrass A G, Rapp A D and Wodzicki K R 2018 *Curr. Clim. Change Rep.* **4** 355–70
[52] Chou C, Wu T C and Tan P H 2013 *Clim. Dyn.* **41** 2481–96
[53] Kroll C A, Dacie S, Azoulay A, Schmidt H and Timmreck C 2020 *Atmos. Chem. Phys. Discuss.* 1–45
[54] Joseph R and Zeng N 2011 *J. Clim.* **24** 2045–60
[55] Man W, Zhou T and Jungclaus J H 2014 *J. Clim.* **27** 7394–409
[56] Zuo M, Man W and Zhou T 2021 *J. Clim.* **34** 8273–89
[57] Pausata F S R, Zanchettin D, Karamperidou C, Caballero R and Battisti D S 2020 *Sci. Adv.* **6** eaaz5006
[58] Rao M P *et al* 2017 *Geophys. Res. Lett.* **44** 5104–12
[59] Tejedor E, Steiger N J, Smerdon J E, Serrano-Notivoli R and Vuille M 2021 *Proc. Natl Acad. Sci.* **118** e2019145118
[60] Erez M and Adam O 2021 *J. Clim.* 1–58
[61] Bhardwaj A, Kaur J, Wuest M Wuest F 2017 *Nat. Commun.* **8** 1–13
[62] Stevenson S, Otto-Bliesner B, Fasullo J and Brady E 2016 *J. Clim.* **29** 2907–21
[63] Paik S, Min S-K, Iles C E, Fischer E M and Schurer A P 2020 *Sci. Adv.* **6** eaba1212
[64] Shukla J and Paolino D A 1983 *Mon. Weather Rev.* **111** 1830–7
[65] Colose C M, LeGrande A N and Vuille M 2016 *Earth Syst. Dyn.* **7** 681–96
[66] Liu F, Chai J, Wang B, Liu J, Zhang X and Wang Z 2016 *Sci. Rep.* **6** 1–11
[67] Zambri B and Robock A 2016 *Geophys. Res. Lett.* **43** 20–8
[68] Fiedler S *et al* 2020 *Mon. Weather Rev.* **148** 3653–80
[69] Anchukaitis K, Buckley B, Cook E, Cook B, D'Arrigo R and Ammann C 2010 *Geophys. Res. Lett.* **37**
[70] Alfaro-Sánchez R, Nguyen H, Klesse S, Hudson A, Belmecheri S, Köse N, Diaz H, Monson R, Villalba R and Trouet V 2018 *Nat. Geosci.* **11** 933–8
[71] Zanchettin D *et al* 2022 *Geosci. Model Dev.* **15** 2265–92
[72] Zanchettin D *et al* 2016 *Geosci. Model Dev.* **9** 2701–19